

# On the morphology of dust lanes in galactic bars

L. Sánchez-Menguiano,<sup>1,2</sup> I. Pérez,<sup>2</sup> A. Zurita,<sup>2</sup> I. Martínez-Valpuesta,<sup>3,4</sup>  
J. A. L. Aguerri,<sup>3</sup> S. F. Sánchez,<sup>5</sup> S. Comerón,<sup>6,7</sup> and S. Díaz-García<sup>6</sup>

<sup>1</sup>*Instituto de Astrofísica de Andalucía (CSIC), Glorieta de la Astronomía s/n, Aptdo. 3004, E-18080 Granada, Spain*

<sup>2</sup>*Dpto. de Física Teórica y del Cosmos, Universidad de Granada, Facultad de Ciencias (Edificio Mecenas), E-18071 Granada, Spain*

<sup>3</sup>*Instituto de Astrofísica de Canarias, E-38205 La Laguna, Tenerife, Spain*

<sup>4</sup>*Universidad de La Laguna, Dpto. Astrofísica, E-38206 La Laguna, Tenerife, Spain*

<sup>5</sup>*Instituto de Astronomía, Universidad Nacional Autónoma de México, A.P. 70-264, 04510, México, D.F.*

<sup>6</sup>*University of Oulu, Astronomy Division, Department of Physics, P.O. Box 3000, FI-90014, Finland*

<sup>7</sup>*Finnish Centre of Astronomy with ESO (FINCA), University of Turku, Väisälänti 20, FI-21500, Piikkiö, Finland*

Accepted 2015 April 7. Received 2015 April 6; in original form 2014 December 9

## ABSTRACT

The aim of our study is to use dynamical simulations to explore the influence of two important dynamical bar parameters, bar strength and bar pattern speed, on the shape of the bar dust lanes. To quantify the shape of the dust lanes we have developed a new systematic method to measure the dust lane curvature. Previous numerical simulations have compared the curvature of bar dust lanes with the bar strength, predicting a relation between both parameters which has been supported by observational studies but with a large spread. We take into account the bar pattern speed to explore, simultaneously, the effect of both parameters on the dust lane shape. To that end, we separate our galactic bars in fast bars ( $1 < \mathcal{R} < 1.4$ ) and slow bars ( $\mathcal{R} > 1.4$ ), obtaining, as previous simulations, an inverse relation between the dust lane curvature and the bar strength for fast bars. For the first time, we extend the study to slow bars, finding a constant curvature as a function of the bar strength. As a result, we conclude that weak bars with straight dust lanes are candidates for slow bars. Finally, we have analysed a pilot sample of ten S<sup>4</sup>G galaxies, obtaining dust lane curvatures lying within the range covered by the simulations.

**Key words:** methods: numerical – methods: observational – galaxies: kinematics and dynamics – galaxies: structure – galaxies: spiral.

## 1 INTRODUCTION

Bars are common morphological features among spiral galaxies. Roughly 30–40% of the spiral galaxies have a pronounced bar in optical wavelengths and if we take into account weaker bars, the fraction rises up to 60% (de Vaucouleurs 1963; Sellwood & Wilkinson 1993; Marinova & Jogee 2007; Barazza, Jogee & Marinova 2008; Sheth et al. 2008; Aguerri, Méndez-Abreu & Corsini 2009; Nair & Abraham 2010; Masters et al. 2011). Kinematic data shows the presence of strong non-circular gas motions in bars (e.g. Huntley 1978; Zurita et al. 2004), which indicates that the bar constitutes a major non-axisymmetric component of the galaxy mass distribution (Sellwood & Wilkinson 1993).

Stellar bars are thought to be a key mechanism in the dynamical evolution of disc galaxies. For example, they are able to contribute to the redistribution of matter in the galaxy by exchanging angular momentum with the disc, bulge and halo (e.g. Debattista & Sellwood 1998, 2000; Athanassoula 2003; Cheung et al. 2013 and reviews by Kor-

mendy & Kennicutt 2004; Athanassoula 2013 and Sellwood 2014).

Galactic bars are characterised dynamically by three main parameters: length, strength<sup>1</sup> and pattern speed. Several methods have been proposed to measure them. Determining the bar length is not entirely trivial. For instance, early-type galaxies do not usually have obvious spiral structure that demarcates the bar end. In other cases, the presence of a large bulge may also complicate the measurement. For example, Aguerri, Debattista & Corsini (2003) applied four different criteria to determine the bar length, which leads to variations of  $\sim 15$ –20% in measured length<sup>2</sup>. Visual inspection of galaxy images (e.g. Martin 1995), ellipse fitting of the isophotes by locating the maximum in the ellipticity

<sup>1</sup> Parameter that quantifies the effectiveness to which a bar potential influences the motions of stars.

<sup>2</sup> Based on the mean values and standard deviations from their Table 4.

profile (e.g. Wozniak & Pierce 1991) or by looking for variations of the position angle (e.g. Wozniak et al. 1995; Aguerri et al. 2009) and Fourier analysis of the surface brightness (e.g. Ohta, Hamabe & Wakamatsu 1990; Aguerri, Beckman & Prieto 1998; Aguerri et al. 2000) are among the several methods proposed for measuring the bar length. For details on different techniques and definitions used to determine the bar length see, for instance, Michel-Dansac & Wozniak (2006) and Gadotti et al. (2007). Studies have obtained a typical value for the bar length of 6-8 kpc, being bars longer by a factor of  $\sim 2.5$  in early-type disc galaxies than in late-type disc galaxies (Erwin 2005).

Regarding bar strength, different parameters have been proposed to describe it. One of the simplest is the deprojected bar ellipticity (Martin 1995). Combes & Sanders (1981) proposed a parameter  $Q_b$  which represents the maximum bar torque applied to a gaseous material in orbital motion relative to its specific kinetic energy. This is one of the most frequently used parameters to describe bar strength. Fourier techniques are also commonly used to measure the bar torque (e.g. Aguerri et al. 2000; Buta, Block & Knapen 2003; Martínez-Valpuesta, Shlosman & Heller 2006).

The bar pattern speed is one of the most defining dynamical parameters. It can be parametrised by a distance-independent parameter  $\mathcal{R} = R_{\text{CR}}/R_{\text{bar}}$ , where  $R_{\text{CR}}$  is the Lagrangian/corotation radius and  $R_{\text{bar}}$  is the bar semimajor axis. Bars that end near corotation ( $1 < \mathcal{R} < 1.4$ ) are considered as fast bars and shorter bars ( $\mathcal{R} > 1.4$ ) as slow bars (Debattista & Sellwood 2000). For  $\mathcal{R} < 1$ , orbits are elongated perpendicular to the bar and self-consistent bars cannot exist (Contopoulos 1980). The bar pattern speed is also difficult to measure. Several methods are usually used to determine it, but the uncertainties in the analysis give inconclusive results (Knapen 1999). The most direct determination is by applying the Tremaine-Weinberg method, based on the continuity equation (Tremaine & Weinberg 1984), but it requires imaging data with high signal-to-noise and, therefore, long integration times, which limits its application to a restricted number of candidates (e.g. Debattista, Corsini & Aguerri 2002; Gerssen, Kuijken & Merrifield 2003; Aguerri et al. 2003; Treuthardt et al. 2007). Aguerri et al. (2015) has applied this method to a larger sample of galaxies taking advantage of integral field spectroscopy data from the CALIFA survey (Sánchez et al. 2012), not finding differences of pattern speed with morphological types. Recent work (Font et al. 2014) has presented a new direct method to locate resonances in a disc using 2-D gas information. It requires high velocity and spatial resolution of ionised gas data. They find that most of the analysed bars are consistent with being fast and present a hint of pattern speed segregation with morphological types.

These properties of bars determine their influence in the galactic dynamics and produce or modify some morphological features. Due to the difficulties in determining these bar parameters, it is highly desirable to find indirect methods to derive them, like the use of morphological information of the bar. Previous studies have derived the bar pattern speed matching observational features with resonances, for instance using rings as indicators (e.g. Buta 1986), even for galaxies at high redshift (Pérez, Aguerri & Méndez-Abreu 2012). One of the most remarkable features of bars is the presence of dust lanes along them that extend from the

nuclear region into the spiral arms. Bar dust lanes have been studied from numerical simulations (e.g. van Albada & Sanders 1982; Athanassoula 1992; Patsis & Athanassoula 2000; Patsis, Kalapotharakos & Grosbøl 2010; Kim, Seo & Kim 2012), as well as observationally (e.g. Knapen, Pérez-Ramírez & Laine 2002; Marshall et al. 2008; Comerón et al. 2009). These show different morphologies; from completely straight, although they can sometimes curl around the centre, to curved, with the concave sides towards the major axis.

Studies of gas flows in bars (mainly theoretically from N-body simulations, e.g. Fux 1999; Pérez, Fux & Freeman 2004; Pérez 2008) have shown that dust lanes are sites of high gas and dust density, and therefore, of high absorption of the starlight. Numerical simulations (Athanassoula 1992; Patsis et al. 2010) have revealed the existence of shocks at the positions of these narrow lanes. The existence of shocks along the dust lanes has been observationally shown from the analysis of gas kinematics of strongly barred galaxies (e.g. Downes et al. 1996; Mundell & Shone 1999; Zurita et al. 2004). These shocks are tracing the channels by which the gas flows towards the galaxy centres where it can contribute to the central mass concentration, for example producing star formation, pseudo-bulges formation or AGN activity (e.g. Shlosman, Frank & Begelman 1989; Oh, Oh & Yi 2012; Wang et al. 2012; Lee et al. 2012).

Numerical simulations have pointed out a relation between the shape of the dust lanes and the bar strength, where stronger bars show straighter dust lanes, and between the position of the dust lanes and the bar pattern speed, where dust lanes that are offset from the bar major axis appear for a limited range of bar pattern speeds, below which the dust lanes are ‘centred’ (Athanassoula 1992). There have been a few attempts to observationally find this relation between dust lane curvature and bar strength (Knapen et al. 2002; Comerón et al. 2009), but without taking into account the bar pattern speed. Even though Knapen et al. (2002) confirmed a correlation between bar strength and dust lane curvature, Comerón et al. (2009), using a larger sample and improving the number statistics from Knapen et al. (2002), showed a large spread in the data and concluded that, though bar strength set an upper limit to the dust lane curvature allowed, this parameter by itself did not determine the dust lane curvature.

In this paper we use dynamical simulations to explore the effect of bar strength and bar pattern speed on the shape of the bar dust lanes. To carry out this study we have developed a new methodology to characterise the dust lane shapes based on the mathematical definition of curvature on a set of simulated galaxies. The final aim of the work would be to derive information about the underlying dynamics of bars by a simple analysis of morphological features, with easier measurements.

The structure of the paper is organised as follows. In Section 2, we provide a description of the simulations used in this study. In Section 3, we explain the methodology developed to measure the bar dust lane curvature. In Section 4, we present the results found in this work and analyse the dependency of the curvature on bar parameters. Finally, in Section 5 we discuss the results and compare them with previous studies in this topic.

## 2 DYNAMICAL SIMULATIONS

To study the dynamical response of the gas in the presence of a galactic bar we used an updated version of the FTM 4.4 code from Heller & Shlosman (1994), a three-dimensional hybrid SPH/N-body code. We ran a set of 238 simulations, which were performed with  $10^5$  isothermal, non self-gravitating, collisional particles. These are the same simulations used in Comerón et al. (2009).

The potential used in the simulations consists of three axisymmetric components associated to the galaxy disc, bulge and halo, each one modelled by a Miyamoto-Nagai profile, and a non-axisymmetric component identified with the bar, modelled by a Ferrers potential (Ferrers 1877) with  $n = 1$ , being  $n$  the degree of the central density concentration. The halo and disc masses are constant for all the simulations, but we vary the bulge to total mass ratio,  $B/(B+D)$ , by increasing the bulge mass. We have used in the simulations two different values of the bar mass, being one bar a 50% more massive than the other. For more details about the parameter values used in the potential models, see Comerón et al. (2009).

Regarding the bar pattern speed, we use  $\Omega_b$  equal to 10, 20, 30 and 40 km s<sup>-1</sup> kpc<sup>-1</sup>, placing the corotation radius outside the bar and obtaining values for  $\mathcal{R}$  between 1.0 and 3.34. Bars with  $R_{CR}/R_{bar} > 3.0$  are very rare in nature. Only one is found in the compilation made by Rautiainen et al. (2008), with  $\mathcal{R} = 3.43 \pm 0.95$ , and even in that case the error may still place the value below the limit of 3.0. For this reason, we have discarded those simulations in which corotation radius is more than three times the bar radius. After this, the number of simulations drops to 175.

We derive analytically the bar strength of the simulated galaxies by using the parameter proposed by Combes & Sanders (1981),  $Q_b$ , which is given by the maximum over  $r$  of

$$Q_b = \frac{F_T^{\max}(r)}{\langle F_R(r) \rangle} = \frac{\frac{1}{r} \left| \frac{\partial \Phi(r, \phi)}{\partial \phi} \right|_{\max}}{\langle \frac{d\Phi_0(r)}{dr} \rangle}, \quad (1)$$

where  $r$  is the galactocentric distance,  $F_T^{\max}$  is the azimuthal maximum of the absolute tangential force in the bar region,  $\langle F_R(r) \rangle$  the mean axisymmetric radial force,  $\Phi(r, \phi)$  the in-plane gravitational potential and  $\Phi_0(r)$  its axisymmetric component.

## 3 MEASUREMENT OF THE BAR DUST LANE CURVATURE

A way to characterise and quantify the shape of bar dust lanes is by measuring its curvature. As dust lanes are related to gas shocks, we measure their curvature in our set of simulated galaxies by deriving the curvature of the gas density enhancements, using a systematic and easily reproducible method, explained below. The range we cover to measure the dust lane curvature starts outside the bar inner region, defined by the nuclear ring associated to the ILR in some cases, or a ring without closure in others, and finishes at the beginning of spiral arms, corresponding to a kink in the dust lane direction. This measurement was performed after two bar rotations in the simulations. Well-defined measurable dust lanes appeared in 126 simulations. This final sample

does not exactly match the sample in Comerón et al. (2009), which comprises 88 simulations. Regrettably, it is not possible to access the sample presented in Comerón et al. (2009), and therefore, we cannot check the source of the discrepancy in the number of galaxies.

To measure the curvature we visually trace one of the dust lanes in each simulation (in our simulations both dust lanes are symmetrical) making use of SAOImage ds9<sup>3</sup>. Figure 1 shows the outline of a dust lane in three simulated galaxies. Then we fit the points tracing the bar dust lane with a third degree polynomial (Figure 1). To check the goodness of the fit we calculate the medium residuals of the fit for each galaxy, which is a measure of the discrepancy between the data and the model. Performing this test, the mean value of the residuals for all galaxies is of 0.2 pixels<sup>4</sup>, with a standard deviation of 0.1 pixels, which reflects that a third degree polynomial fits quite well the data. In the particular case of the simulated galaxies shown in Figure 1, from left to right the maximum residual for each fitting is 0.43, 0.16 and 0.69 pixels, with a mean residual along the fitting of 0.18, 0.08 and 0.38 pixels, respectively.

From the fitting of the bar dust lanes we now measure their curvature. The curvature of a plane curve gives information on how fast its tangent vector changes direction as you travel along the curve, and this is exactly what we want to know about the bar dust lane shape. If the dust lane keeps close to the same direction (that is, the dust lane is straight), the unit tangent vector changes very little and the curvature is small (the opposite if the dust lane undergoes a tight turn). To measure bar dust lane curvature we use the mathematical definition of curvature for a plane curve written in cartesian coordinates in the form  $y = f(x)$

$$\kappa \equiv \frac{d\phi}{ds} = \frac{|y''(x)|}{(1 + (y'(x))^2)^{3/2}} \quad (2)$$

where  $\phi$  is the tangential angle and  $s$  is the arc length. It has units of inverse distance. For more details about the mathematical deduction of the curvature of a function see, for example, Weisstein (2003).

We should not forget that this mathematical curvature is not a constant function. Therefore, we have adopted as ‘curvature of a bar dust lane’ the absolute mean value of the curvature along the bar dust lane. This parameter is zero for straight bar dust lanes and progressively increases as these deviate from straight lines.

Besides, we should also notice that the curvature, as defined before, is a measurement that depends on the absolute bar size. As in the simulations this parameter is constant, we do not have to deal with this issue. However, to apply this method to observational data, we need to ‘normalise’ the curvature to obtain a dimensionless parameter which takes into account the size of the bars, multiplying the mean curvature by the bar semimajor axis.

To show that the method is viable and easy to implement on observational studies, we have applied it to

<sup>3</sup> An astronomical imaging and data visualisation application developed by Smithsonian Astrophysical Observatory (Joye & Mandel 2003).

<sup>4</sup> Taking the unit length of simulations to 10 kpc, each pixel corresponds to 60 pc.

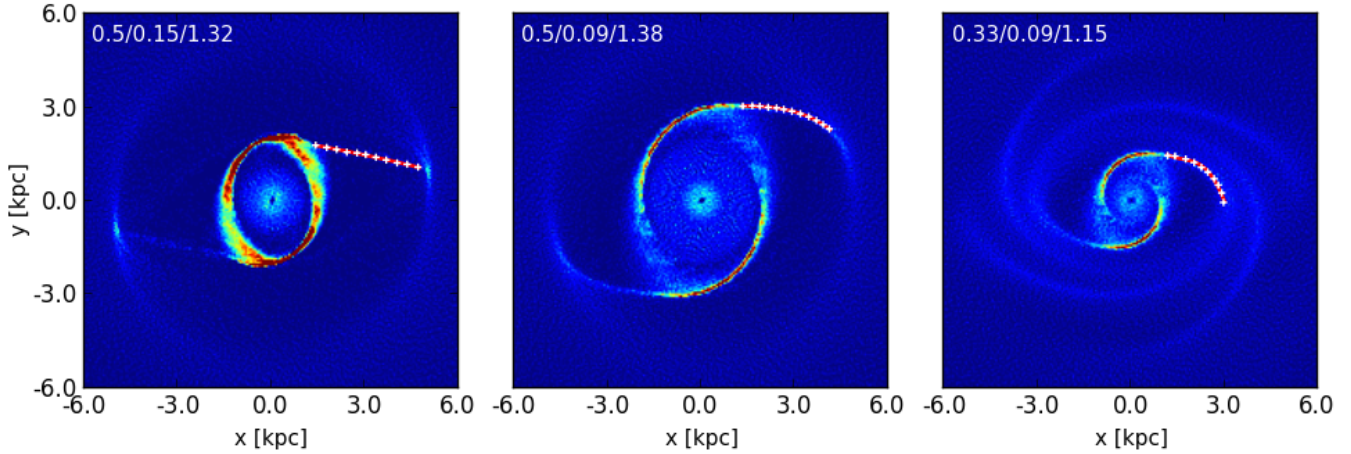


**Figure 1.** Gas density maps of the bar region for three simulated galaxies with one of the dust lanes marked (white crosses). Bar major axis is parallel to the horizontal in all frames. We have also plotted the dust lane fitting using a third degree polynomial (red line), see text for details. Ellipticity, bar strength and the ratio of corotation radius to bar semimajor axis ( $\mathcal{R}$ ) are given in this order in the upper left-hand corner of each frame. From left to right, the dust lane curvatures (as explained in Sect. 3) are 1.0, 1.3 and 2.3.

a pilot sample. This sample comprises the galaxies from Comerón et al. (2009) for which there are measurements of their bar pattern speed in Rautiainen et al. (2008).  $Q_b$  values are taken from Díaz-García et al. (in prep), who inferred the gravitational potential from the  $3.6 \mu\text{m}$  imaging of the Spitzer Survey of Stellar Structure in Galaxies sample ( $S^4G$ )<sup>5</sup> following the recipe from Laurikainen & Salo (2002) and Salo et al. (2010). To obtain the curvature values, we have followed the same procedure as for the simulations, using  $g$  or colour-index  $g - r$  images, proxies for dust distribution, from SDSS when available and otherwise, other optical images from the NASA / IPAC Extragalactic Database (NED). Table 1 shows the names of the galaxies included in the study, as well as some of their properties and the derived normalised curvatures, for both bar dust lanes when possible, and just for one when the other is not well-defined.

## 4 RESULTS

We want to assess the influence of bar strength and bar pattern speed on the curvature of bar dust lanes. For that purpose, we have developed in this work a new methodology to quantitatively measure bar dust lane curvatures (see Section 3).

In Figure 2 we show the derived dust lane curvatures as a function of the bar ellipticity distinguishing between fast ( $1 < \mathcal{R} < 1.4$ ) and slow ( $\mathcal{R} > 1.4$ ) bars. The red stars are the mean curvature values for each ellipticity. The blue circular markers are the values for galaxies with a bar mass of  $M_b = 1.0 \times 10^{10} M_\odot$  and the yellow squares for  $M_b = 1.5 \times 10^{10} M_\odot$ . Finally, the purple triangles are the values for the real galaxies included in the study. In the cases in which it has been possible to measure both dust lanes, they are distinguished using both filled and unfilled markers.

Regarding the mean curvature values, it is clear that for fast bars the curvature is smaller for higher ellipticity values,

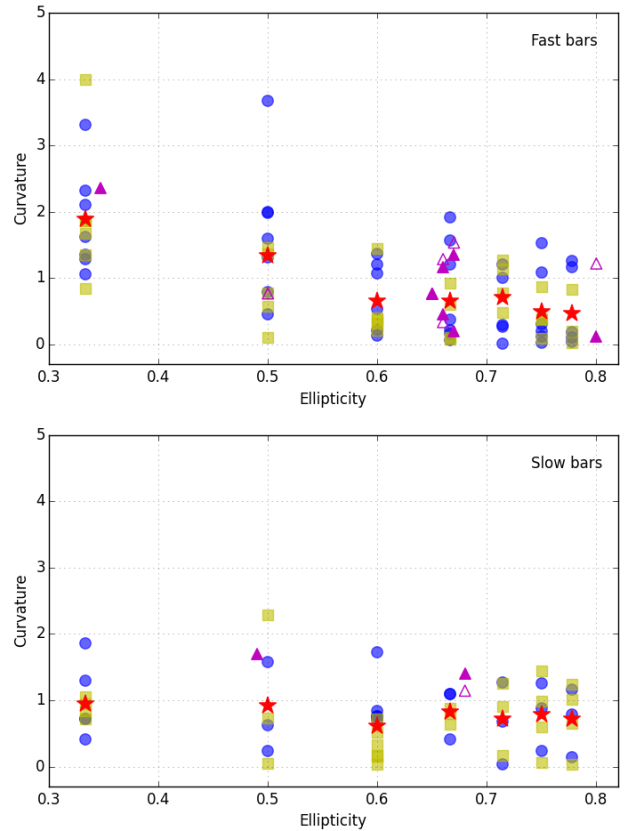


**Figure 2.** Dust lane curvatures as a function of the bar ellipticity  $\epsilon$  for fast bars, i.e.,  $1 < \mathcal{R} < 1.4$  (upper) and for slow bars, i.e.,  $\mathcal{R} > 1.4$  (bottom). The red stars mark the medium value of curvature for each value of the ellipticity. The blue circular markers are the values for galaxies with a bar mass of  $M_b = 1.0 \times 10^{10} M_\odot$  and the yellow squares for  $M_b = 1.5 \times 10^{10} M_\odot$ . The purple triangles correspond to the values for the real galaxies.

<sup>5</sup> <http://www.cv.nrao.edu/~ksheth/S4G/>

**Table 1.** Properties of the real galaxies used in the study.

Name (NGC)	$i_d$ (deg)	$PA_d$ (deg)	$\mathcal{R}$	$a_b$ (kpc)	$\varepsilon_b$	$Q_b$	$\kappa$
3504	20.93	138.3	1.19	4.20	0.63	0.26	1.35/1.54
4123	39.45	119.9	1.17	4.52	0.65	0.57	0.77/0.77
4303	24.77	153.0	1.70	6.36	0.68	0.42	1.40/1.14
4314	22.78	42.7	0.99	6.63	0.67	0.45	0.20
4457	17.64	69.7	0.98	2.60	0.35	0.09	2.37
4548	31.46	144.2	1.26	5.88	0.61	0.28	0.46/1.29
4579	43.20	96.5	1.46	6.05	0.49	0.18	1.70
5921	39.48	120.3	1.25	5.82	0.80	0.36	0.12/1.22
7552	15.63	26.0	0.99	4.84	0.66	0.36	1.16/0.34
7723	44.30	47.1	1.31	2.81	0.50	0.27	0.77

The table shows the galaxy name (Column 1), the galaxy disc inclination and disc PA (Columns 2 and 3) from Muñoz-Mateos et al. (2013), the bar pattern speed parametrised by  $\mathcal{R}$  from Rautiainen et al. (2008) (Column 4), the deprojected bar semi-major axis and ellipticity (Columns 5 and 6) from Muñoz-Mateos et al. (2013), the bar strength (Column 7) from Díaz-García et al. (in preparation) and the dust lane curvature measured as defined in Section 3 (Column 8).

and slow bars show similar values of the mean curvature for all ellipticity values. There seems to be a lack of points for fast bars at low ellipticities and low curvatures, this effect is not so evident for slow bars. The most striking result from this figure is the absence of high curvature points for slow bars. In fact, the average curvature value for slow bars at the lowest ellipticity is 0.95 while the value for fast bars is 1.90. We show later in this section that the distribution of points for both fast and slow bars is clearly different. As it can be seen from Figure 2, the values for the real galaxies are within the range of parameters covered by the simulations.

Figure 3 presents the curvature against the bar strength, again distinguishing between fast (top panel) and slow bars (bottom panel). The marker symbols and colours used are the same as in the previous figure, being the red stars the mean curvature values for bar strength bins of 0.1.

We observe similar trends to those found in Figure 2, indicating that, in this case, the ellipticity is a good proxy for bar strength. Previous studies comparing bar strength and ellipticity for a large sample of galaxies have reached a similar conclusion (e.g. Laurikainen, Salo & Rautiainen 2002). For slow bars, we have almost constant curvature value for the whole range of bar strengths while for fast bars we found higher curvature values at low bar strength. As shown in Figure 2, there is a lack of low curvature points for fast bars at low bar strengths and a deficit of high curvature points for slow bars. Also in this case, the values for the real galaxies are within the range of parameters covered by the simulations.

We perform a two-sample Kolmogorov-Smirnov test to check if the differences found in the results between fast and slow bars are statistically significant, obtaining a P-value of 12%. The significance level of the K-S test is 5%, meaning that values below this limit come from different distributions. Therefore, the two complete samples seem to have similar distributions. However, if we restrict the comparison range to weak bars, with  $Q_b \leq 0.3$ , where we observe differences between both distributions, the P-value is now 2%.

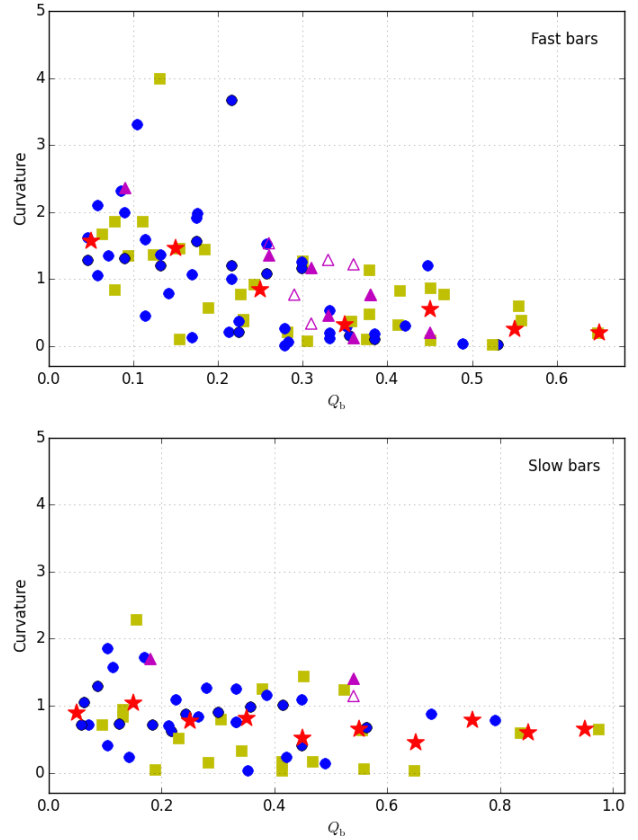


**Figure 3.** Dust lane curvatures as a function of the bar strength  $Q_b$  for fast bars, i.e.,  $1 < \mathcal{R} < 1.4$  (upper) and for slow bars, i.e.,  $\mathcal{R} > 1.4$  (bottom). The red stars are the medium values of the curvature for ranges of the bar strength of 0.1. The blue circular markers are the values for galaxies with a bar mass of  $M_b = 1.0 \times 10^{10} M_\odot$  and the yellow squares for  $M_b = 1.5 \times 10^{10} M_\odot$ . The purple triangles correspond to the values for the real galaxies.

This result indicates that slow and fast bars have a different distribution of curvature for this range of  $Q_b$  values. At low bar strengths, the statistics of our sample is considerably reduced ( $\approx 30$  elements). Because of this we have also performed an Anderson-Darling test, more appropriate for small samples, obtaining a P-value of 5%, reinforcing the observed trends.

## 5 DISCUSSION AND CONCLUSIONS

In this work we have used numerical simulations to explore the effect of two bar parameters, bar strength and bar pattern speed, on the bar dust lane shape. To characterise the shape of dust lanes, we have developed a new method based on the mathematical curvature of a plane curve, providing a measurement which quantifies this shape, and we have then used these measurements to study the influence of the bar parameters. To do that, we have analysed 126 barred simulations, covering bar strengths from 0 to 1 and  $\mathcal{R}$  between 1.0 and 3.0 for two bar masses. We have also applied this method to a set of observational data.

Athanassoula (1992) studied the shape of bar dust lanes and its dependency on a set of model parameters, like the

Lagrangian radius, the axial ratio of the bar and the bar quadrupole momentum  $Q_m$  as a measurement of the bar mass. However, the characterisation she made of the shape of the dust lanes was purely visual, not providing a method to quantify its curvature and it is therefore difficult to directly apply on observations.

Athanassoula (1992), analysing simulations for fast bars, deduced that curved dust lanes result from weak bars and straight ones originate from strong bars. Our simulation results confirm this prediction. We extend the study to slow bars and find that the curvature does not vary with bar strength. Athanassoula (1992) also included in the study the influence of the bar pattern speed, but more related to the position of the dust lanes than to the shape, which is the purpose of this work. She found a tight range of Lagrangian radii, which corresponds to fast bars in the distinction we have made, that leads to dust lanes that are ‘offset’ from the bar major axis. For smaller values, corresponding to slow bars, the dust lanes are ‘centred’ and for larger values they turn their convex sides towards the bar major axis, corresponding to unrealistic dust lanes.

A methodology similar to the one presented here, is used by Knapen et al. (2002) and Comerón et al. (2009) on real galaxies. These works also developed a way to quantify the curvature of dust lanes using real galaxies. Their method is based on measurements of the change in the angle of the tangent to the curved dust lanes in the range where the curvature is constant, Knapen et al. (2002) expressing the result in units of degrees per kpc and Comerón et al. (2009) multiplying that angle by the angular radius at which the torque is maximal, to take into account the size of the host bars. This method has the advantage of being simple and rather straightforward, but it also presents a number of drawbacks. First, it depends a lot on which part of the dust lane is selected to measure the curvature; and therefore, it is not easy to replicate their results. And second, they also assume a constant curvature for the bar dust lanes, which is not always the case (52% of our simulations show dust lanes with non-constant curvature).

Our methodology does not assume any a priori shape for the dust lanes and the results are easy to reproduce. We select the beginning and end of the dust lanes in such way that we avoid morphological structures, such as nuclear rings and spiral arms, that may be masking the actual dust lane curvature. As we discussed in Sect. 3, we define the end of the dust lane as a kink in the dust lane direction which corresponds to the beginning of the spiral arms. For most of the galaxies, this parameter ranges within a similar galactocentric radius, indicating that our method measures dust lanes close to the bar ends in almost all cases. We have checked the effect of shortening the dust lanes in the curvature determination to test those cases where the dust lanes do not reach the end of the bar. We have done this test on 40 galaxies obtaining that the mean curvature is only changed by 19% on average.

Knapen et al. (2002) results agree with the correlation between the dust lane curvature and the bar strength found by Athanassoula (1992). However, Comerón et al. (2009), using a larger sample, obtained a large spread in the relation that made them state that bar strength by itself did not determine the dust lane curvature.

None of these observational studies take into account

the bar pattern speed as an important parameter influencing the bar dust lane shapes. However, numerical simulations (e.g. van Albada & Sanders 1982; Athanassoula 1992; Fux 1999; Pérez et al. 2004; Pérez 2008) have shown that the location of gas shocks is linked to the bar potential and the pattern speed. We take a step forward adding to the distribution of bar strengths a segregation with bar pattern speed, dividing the sample in fast and slow bars, to find a relation between both parameters and dust lane curvature. The result obtained in the performed Kolmogorov-Smirnov test supports our assumption that the bar pattern speed has influence in the shape of bar dust lanes. We find that this inverse relation between the dust lane curvature and the bar strength only holds for fast bars, obtaining for slow bars approximately a constant curvature for all the values of the bar strength.

The distribution of points shown in Figure 3 indicates a larger probability of finding slow bars among galaxies with weak bars and straight dust lanes. This is an interesting effect to be checked observationally.

We have tested this method on a set of S<sup>4</sup>G galaxies for which we have pattern speed and bar strength measurements. We have followed the same procedure as described for the simulations. Despite the fact that the sample is not large enough to confirm the trends found here, the obtained values lie within the range of values covered by the simulations.

Although all parameters have been measured in a similar way for both simulations and observations, the halo potential is not included in the measurement of the bar strength in the S<sup>4</sup>G galaxies. In principle, this could modify the results since the dust lane morphology depends on the whole galaxy potential. However, the analysed sample is comprised of high surface brightness galaxies for which is commonly assumed a maximum disc, implying that the contribution of the dark halo in the optical disc is minimum (e.g. van Albada & Sancisi 1986; Broeils 1992; Weiner, Sellwood & Williams 2001; Pérez et al. 2004). Because of this we do not expect the results to be substantially changed. Furthermore, the fact that the bar strength follows the ellipticity trend also reinforces this assumption.

In summary, we have developed a method to measure dust lane curvatures that is robust and easily applicable to observational data. A future work using a larger sample of galaxies with measurements of bar strength and pattern speed is necessary to test the trends found with the simulations.

## ACKNOWLEDGEMENTS

We acknowledge financial support from the Spanish *Ministerio de Economía y Competitividad* via grants AYA2011-24728 and AYA2012-31935, and from the ‘Junta de Andalucía’ local government through the FQM-108 project. We also acknowledge support to the DAGAL Network from the People Programme (Marie Curie Actions) of the European Union’s Seventh Framework Programme FP7/2007-2013/ under REA grant agreement number PITN-GA-2011-289313.

## REFERENCES

- Aguerri J. A. L., Beckman J. E., Prieto M., 1998, *AJ*, 116, 2136
- Aguerri J. A. L., Debattista V. P., Corsini E. M., 2003, *MNRAS*, 338, 465
- Aguerri J. A. L., et al., 2015, *ArXiv e-prints*
- Aguerri J. A. L., Méndez-Abreu J., Corsini E. M., 2009, *A&A*, 495, 491
- Aguerri J. A. L., Muñoz-Tuñón C., Varela A. M., Prieto M., 2000, *A&A*, 361, 841
- Athanassoula E., 1992, *MNRAS*, 259, 345
- Athanassoula E., 2003, *MNRAS*, 341, 1179
- Athanassoula E., 2013, *Bars and secular evolution in disk galaxies: Theoretical input.* p. 305
- Barazza F. D., Jogee S., Marinova I., 2008, in Funes J. G., Corsini E. M., eds, *Formation and Evolution of Galaxy Disks Vol. 396 of ASP Conf. Ser.*, *Bars in Local Galaxies: Evidence for a Higher Optical Bar Fraction in Disk-Dominated Galaxies.* p. 351
- Broeils A. H., 1992, *Dark and visible matter in spiral galaxies*
- Buta R., 1986, *ApJS*, 61, 609
- Buta R., Block D. L., Knapen J. H., 2003, *AJ*, 126, 1148
- Cheung E., et al., 2013, *ApJ*, 779, 162
- Combes F., Sanders R. H., 1981, *A&A*, 96, 164
- Comerón S., Martínez-Valpuesta I., Knapen J. H., Beckman J. E., 2009, *ApJ*, 706, L256
- Contopoulos G., 1980, *A&A*, 81, 198
- de Vaucouleurs G., 1963, *ApJ*, 8, 31
- Debattista V. P., Corsini E. M., Aguerri J. A. L., 2002, *MNRAS*, 332, 65
- Debattista V. P., Sellwood J. A., 1998, *ApJ*, 493, L5
- Debattista V. P., Sellwood J. A., 2000, *ApJ*, 543, 704
- Downes D., Reynaud D., Solomon P. M., Radford S. J. E., 1996, *ApJ*, 461, 186
- Erwin P., 2005, *MNRAS*, 364, 283
- Ferrers N. M., 1877, *Q. J. Pure Appl. Math.*, 14, 1
- Font J., Beckman J. E., Querejeta M., Epinat B., James P. A., Blasco-herrera J., Erroz-Ferrer S., Pérez I., 2014, *ApJS*, 210, 2
- Fux R., 1999, *A&A*, 345, 787
- Gadotti D. A., Athanassoula E., Carrasco L., Bosma A., de Souza R. E., Recillas E., 2007, *MNRAS*, 381, 943
- Gerssen J., Kuijken K., Merrifield M. R., 2003, *MNRAS*, 345, 261
- Heller C. H., Shlosman I., 1994, *ApJ*, 424, 84
- Huntley J. M., 1978, *ApJ*, 225, L101
- Joye W. A., Mandel E., 2003, in Payne H. E., Jedrzejewski R. I., Hook R. N., eds, *Astronomical Data Analysis Software and Systems XII Vol. 295 of ASP Conf. Ser.*, *New Features of SAOImage DS9.* p. 489
- Kim W.-T., Seo W.-Y., Kim Y., 2012, *ApJ*, 758, 14
- Knapen J. H., 1999, in Beckman J. E., Mahoney T. J., eds, *The Evolution of Galaxies on Cosmological Timescales Vol. 187 of ASP Conf. Ser.*, *Observations of Barred Galaxies.* pp 72–87
- Knapen J. H., Pérez-Ramírez D., Laine S., 2002, *MNRAS*, 337, 808
- Kormendy J., Kennicutt J. R. C., 2004, *ARA&A*, 42, 603
- Laurikainen E., Salo H., 2002, *MNRAS*, 337, 1118
- Laurikainen E., Salo H., Rautiainen P., 2002, *MNRAS*, 331, 880
- Lee G.-H., Woo J.-H., Lee M. G., Hwang H. S., Lee J. C., Sohn J., Lee J. H., 2012, *ApJ*, 750, 141
- Marinova I., Jogee S., 2007, *ApJ*, 659, 1176
- Marshall D. J., Fux R., Robin A. C., Reylé C., 2008, *A&A*, 477, L21
- Martin P., 1995, *AJ*, 109, 2428
- Martínez-Valpuesta I., Shlosman I., Heller C., 2006, *ApJ*, 637, 214
- Masters K. L., et al., 2011, *MNRAS*, 411, 2026
- Michel-Dansac L., Wozniak H., 2006, *A&A*, 452, 97
- Muñoz-Mateos J. C., et al., 2013, *ApJ*, 771, 59
- Mundell C. G., Shone D. L., 1999, *MNRAS*, 304, 475
- Nair P. B., Abraham R. G., 2010, *ApJ*, 714, L260
- Oh S., Oh K., Yi S. K., 2012, *ApJ*, 198, 4
- Ohta K., Hamabe M., Wakamatsu K.-I., 1990, *ApJ*, 357, 71
- Patsis P. A., Athanassoula E., 2000, *A&A*, 358, 45
- Patsis P. A., Kalapotharakos C., Grosbøl P., 2010, *MNRAS*, 409, L94
- Pérez I., 2008, *A&A*, 478, 717
- Pérez I., Aguerri J. A. L., Méndez-Abreu J., 2012, *A&A*, 540, A103
- Pérez I., Fux R., Freeman K., 2004, *A&A*, 424, 799
- Rautiainen P., Salo H., Laurikainen E., 2008, *MNRAS*, 388, 1803
- Salo H., Laurikainen E., Buta R., Knapen J. H., 2010, *ApJ*, 715, L56
- Sánchez S. F., et al., 2012, *A&A*, 538, A8
- Sellwood J. A., 2014, *Rev. Modern Phys.*, 86, 1
- Sellwood J. A., Wilkinson A., 1993, *Rep. Prog. Phys.*, 56, 173
- Sheth K., et al., 2008, *ApJ*, 675, 1141
- Shlosman I., Frank J., Begelman M. C., 1989, *Nature*, 338, 45
- Tremaine S., Weinberg M. D., 1984, *ApJ*, 282, L5
- Treuthardt P., Buta R., Salo H., Laurikainen E., 2007, *AJ*, 134, 1195
- van Albada T. S., Sancisi R., 1986, *R. Soc. Long. Philos. Trans. Royal Society of London Philosophical Transactions Series A*, 320, 447
- van Albada T. S., Sanders R. H., 1982, *MNRAS*, 201, 303
- Wang J., et al., 2012, *MNRAS*, 423, 3486
- Weiner B. J., Sellwood J. A., Williams T. B., 2001, *ApJ*, 546, 931
- Weisstein E. W., 2003, *CRC Concise Encyclopedia of Mathematics, Second Edition* edn. Chapman & Hall/CRC
- Wozniak H., Friedli D., Martinet L., Martin P., Bratschi P., 1995, *A&AS*, 111, 115
- Wozniak H., Pierce M. J., 1991, *A&AS*, 88, 325
- Zurita A., Relaño M., Beckman J. E., Knapen J. H., 2004, *A&A*, 413, 73